Publication status: Not informed by the submitting author

Cellulose nanocrystals as additives in Nafion membranes for water electrolysis applications

Jéssica de Aguiar, Marcelo Carmo, Caue Ribeiro de Oliveira, Luiz Henrique Capparelli Mattoso, José Manoel Marconcini

https://doi.org/10.1590/SciELOPreprints.4294

Submitted on: 2022-06-16
Posted on: 2022-06-23 (version 1)
(YYYY-MM-DD)

Cellulose nanocrystals as additives in Nafion membranes for water electrolysis applications

Jéssica de Aguiar[1], https://orcid.org/0000-0002-4202-9309

Marcelo Carmo[2], https://orcid.org/0000-0002-0186-317X

Cauê Ribeiro de Oliveira[3], https://orcid.org/0000-0002-8908-6343

Luiz Henrique C. Mattoso[1,3] , https://orcid.org/0000-0001-7586-1014

José Manoel Marconcini [1,3] https://orcid.org/0000-0002-0419-9796

[1] Federal University of Sao Carlos, Graduate Program in Materials Science and Engineering, Rodovia Washington Luis, km 235, São Carlos, SP, 13565-905, Brazil

[2] Forschungszentrum Julich GmbH, Julich, Germany

[3] Nanotechnology National Laboratory for Agriculture (LNNA), Embrapa Instrumentation, Rua XV de Novembro, 1452, São Carlos, SP, 13561-206, Brazil

Conflict of interest: The authors have no conflict of interest to disclose.

Author contributions

- *Conceptualization*: Jéssica de Aguiar, Marcelo Carmo, Cauê Ribeiro de Oliveira, José Manoel Marconcini
- *Formal analysis:* Jéssica de Aguiar, Marcelo Carmo, Cauê Ribeiro de Oliveira, José Manoel Marconcini
- *Funding acquisition:* Marcelo Carmo, José Manoel Marconcini, Luiz Henrique C. Mattoso, Cauê Ribeiro de Oliveira
- *Investigation:* Jéssica de Aguiar
- *Methodology:* Jéssica de Aguiar, Marcelo Carmo
- *Project administration:* Jéssica de Aguiar
- *Resources:* José Manoel Marconcini, Marcelo Carmo, Luiz Henrique C. Mattoso, Cauê Ribeiro de Oliveira
- *Supervision:* José Manoel Marconcini, Marcelo Carmo, Luiz Henrique C. Mattoso
- *Writing – original draft:* Jéssica de Aguiar

- Writing – review & editing: Jéssica de Aguiar, José Manoel Marconcini, Luiz Henrique C. Mattoso

ABSTRACT: Proton exchange membrane water electrolysis (PEMWE) performs the electrolysis of water to produce hydrogen, a source of clean and renewable energy. The most used commercial electrolyte in PEMWE is the Nafion membrane, a material that is expensive and difficult to recycle. The partial replacement of Nafion with cellulose nanocrystals (CNCs) can produce composite membranes can increased electrical, mechanical and biodegradability properties. In this sense, the objective of this work is to study the elaboration of nanocomposites (Nafion-CNC) aiming at developing high-performance electrolytes for application in PEMWE. The effects of adding CNCs to Nafion were evaluated. Nafion membranes were produced with two types of CNCs, one obtained by enzymatic hydrolysis and the other by acid hydrolysis (commercial). The addition of both CNCs has similar effects on Nafion's properties. For samples with both commercial and enzymatic CNC, an increase in the modulus of elasticity (10% and 40% respectively) and maximum stress (10% and 13% respectively) was observed. The two nanocomposites showedlower initial thermal degradation temperatures, however, they still showed sufficient stability (Tonset > 170°C) for application in PEMWE (standard operating temperature <100°C). Furthermore, there was a significant increase in the humidification capacity and increase in conductivity. Composite membranes were tested in PEMWE and their usability was proven.

KEYWORDS: Proton Exchange Membrane Water Electrolysis (PEMWE), Cellulose Nanocrystals (CNCs); Nafion;

INTRODUCTION

In recent decades, the need for environmental conservation has become increasingly evident, resulting in a growing search for environmentally friendly materials such as those produced from renewable sources [1]. In this sense, research aimed at the development of new materials has demonstrated the importance of agro-industrial waste as a raw material for the preparation of products with higher added value. The use of these residues besides being economically viable, is also able to minimize environmental problems related to its disposal [2].

Among the various agricultural sectors, sugarcane is known not only for its production volume, but also for its vast waste generation capacity [3]. Currently, Brazil is the largest producer of sugarcane in the world with production between 650 and 700 million tons per year, followed by India (340 million) and China (115 million) [4]. Sugarcane bagasse, a residue of alcohol and sugar production, has been used in the production of second generation ethanol (2G) and has the potential to be used to obtain products of higher added value, such as nanocellulose [5]. In recent studies [6–8] cnc extraction has been explored within the biorefinery concept, since lignocellulosic materials such as sugarcane biomass can be used in a variety of compounds (soluble sugars), structures (micro and nanofibers) [9], biofuels and other bio-based products [10].

Another material from sugarcane production is straw, a residue of the harvesting process, consisting of dried leaves and green tops, kept in the field for soil protection or harvested for bioenergy production [11]. The chemical and morphological properties of straw fibers are similar to those presented by bagasse, making them another potential raw material for the production of

nanocellulose [12]. However, to date, no studies on the use of sugarcane straw to obtain nanocellulose have been found in the literature.

There are different studies investigating the extraction of nanocellulose from sugarcane bagasse. The routes for obtaining these nanostructures mainly include chemical methods [3,13–19], mechanical [20,21] or an association of methods, such as mechanical and enzymatic [22–24]. Nanocellulose has characteristics such as high strength and stiffness, low density, good chemical modification capacity and biodegradability [24,25]. Nanocellulose can be used in the manufacture of nanocomposites, packaging, cosmetics, medical and pharmaceutical products, electronic devices [24,26] and recently in the production of nanocomposites based on Nafion and CNCs for application in fuel cells [27,28].

The presence of large amounts of hydroxyl groups on the surface of nanocellulose is able to ensure a high water absorption capacity, easy functionalization and considerable ability to establish hydrogen bonds with polar polymeric substrates. In the literature, nanocellulose has been investigated for applications where these properties are desired such as photonic films, electrolytic membranes, fuel cells and other related systems [29]. For example, Jiang and [30] collaborators studied film production from bacterial cellulose (BC) and Nafion (through the solvent evaporation forming method) and observed that the materials produced exhibited an increase in ionic conductivity and maintained acceptable thermal stability for applications below 100 °C. In another study, Gadim et al. [28] obtained Nafion membranes with bacterial cellulose (BC) that showed increases in mechanical properties as well as ionic conductivity. In addition, in the work of Hasani-Sadrabad and [31] CNCs collaborators were successfully included in the Nafion membrane to maximize fuel cell performance. The analysis of electrochemical impedance showed that the addition of 5% (m/m) of CNCs can positively affect the protonic conductivity.

However, all these studies have concentrated their efforts to produce nafion and nanocellulose membranes for application in fuel cells. However, the properties presented by these nanocomposites are promising for inclusion in other devices, such as electrolyte cells with proton-changing membrane (PEMECs).

PEMECs are electrochemical devices that perform water electrolysis for hydrogen production. These devices have the potential to revolutionize the energy sector and help society overcome the need to use fossil fuels. PEMECs use water and electric current for hydrogen production without emitting greenhouse gases and have relatively high efficiency [27,32,33].

The basic structure of a PEMEC comprises two porous electrodes, whose composition depends on the type of cell, separated by an electrolyte and connected by an external circuit. The most commonly used membrane is Nafion, which has high proton conductivity (> 100 mS cm-1), good mechanical strength and chemical stability. However, Nafion is an expensive material, difficult to recycle at the end of life, has proton conductivity that relies heavily on humidification and its mechanical stability is compromised at temperatures greater than 100°C [32–34].

In view of the above, it is clear the exploration potential of the properties of nanocomposite electrolytes based on Nafion-CNCs for application in PEMEC. It is also possible to use CNCs obtained from the use of agro-industrial residuas and produced through greener processes such as enzymatic hydrolysis.

EXPERIMENTAL

Chemicals and materials

Nafion solution D1021 as 10 wt% dispersion in water 10 wt% was supplied by Dupont. The freeze-dried Cellulose nanocrystals (CNC) was purchased from the Process Development Center at

University of Maine (USA) and the graphite oxide dispersion (4 mg/mL, dispersion in water) was obtained from Sigma-Aldrich. Other chemicals and solvents were of laboratory grids.

Preparation of pure Nafion and Nafion/CNC membranes

For the elaboration of electrolyte membranes, cellulose nanocrystals obtained by enzymatic route were used from residues of sugarcane production. The protocol for the production of CNCs was defined based on the results observed in the first stage of this study (item 3.1). The method selected is the one that employs enzymatic hydrolysis lasting 72 h in treated fibers of sugarcane straw. This protocol was one of the most promising methods studied because it showed greater balance of properties in relation to aspect ratio, crystalline index and thermal stability.

For the investigation of the properties presented by membranes produced with chemically and morphologically different nanoparticles, membranes with cellulose nanocrystals acquired from the University of Maine were also produced. According to the manufacturer, this commercial CNC has 0.94 % (m/m) of sulphur, diameters between 5 and 20 nm and length between 150 and 200 nm, density of 1.5 g $^{cm-3}$ and hydrophilic surface[35].

Polymeric membranes (100% Nafion) and Nafion nanocomposites containing CNCs (enzymatic or commercial) were produced through the mold evaporation forming technique (*casting*). The membranes were prepared from 10% (m/m) Nafion solution in water (D1021, DuPont). The solvent used in the preparation of polymeric films was dimethylsulfoxide (DMSO, Aldrich, PA).

The production of Nafion membranes by casting has already been studied, evidencing the need for the use of high boiling point solvents, such as dimethylsulxioxide (DMSO). The use of these solvents allows the processing of materials at higher temperatures, promoting a plasticizing

effect thus allowing the production of films with properties similar to commercial membranes [36]. In addition, cellulose nanocrystals have considerable dispersal capacity in mixtures in organic solvents with high dielectric constants, such as DMSO [37,38].

Due to the need for a high boiling point solvent, the water used as a commercial Nafion solvent was replaced through evaporation followed by polymer resolubilization in DMSO. For this, the Nafion solution was maintained at 80 ºC in a beaker on a magnetic stirrer until a viscous residue was obtained. Next, this residue was redissolved in DMSO, obtaining again a solution of 10% (m/m) of Nafion. The solution was kept under magnetic agitation for 24 h. This solution was used in the manufacture of nafion polymeric films without the addition of nanocharges (Ncast) and nanocomposite membranes containing Nafion and 10% (m/m) of commercial CNC (N/CNC_C) and Nafion and 10% (m/m) of enzymatic CNC (N/CNC_ENZ).

As the objective of this work was to perform a partial replacement of the nafion by a biodegradable material, we chose to work with samples containing high concentrations of CNCs. Membranes containing different concentrations of CNCs (10, 15, 25, 50% m/m) were then produced. However, the samples with concentrations of CNCs above 10% (m/m) presented high frailty and were not suitable for application.

For the preparation of the nanocomposites, in addition to the preparation of the Nafion solution in DMSO obtained by the procedure described above, CNC dispersions with the desired mass percentage were prepared using DMSO as dispersant. The CNCs were dispersed in the DMSO using a tip ultrasound operating at 10% amplitude for 15 min, with cooling to avoid overheating. Then, the dispersions were maintained 24 h under mechanical agitation. After this process, nafion solution and CNC dispersions were mixed and maintained under mechanical agitation for 24 h.

Membrane conformation was performed by deposition of CNC/Nafion dispersions in petri dishes for dmso evaporation in a resistive oven. The evaporation process was carried out in two stages, initially the samples were kept at 80 ºC for 18h and then the oven temperature was increased to 120 ºC and maintained for two hours.

After being made, the membranes were washed with deionized water to clean surface impurities and dilute the residual solvent. Next, the sulphonic groups were activation by immersion of the membranes in a sulfuric acid solution (0.5 M) 80 ºC for 1h. Finally, the membranes were washed with deionized water and dried at room temperature.

Physico-chemical characterizations

The analysis of infrared spectroscopy with fourrier transform (FTIR) of the membranes was performed in a Bruker infrared spectrophotometer equipment, model Vertex 70, with ATR accessory (*Attenuated Total Reflectance*). Measurements of total attenuated reflectance were performed with variation of the wave number from 4000 to 650 $^{cm-1}$, resolution of 4 $^{cm-1}$ and 32 spectral accumulations per sample.

X-ray diffatometry analysis was performed on a Shimadzu 6000 diffometer using Cu Kα radiation (λ = 1.54 Å) in continuous scanning mode with a speed of 2º.min-1 in the Bragg angle range (2θ) from 5 to 45º. The samples were cut into squares and fixed with double-sided tape under a glass blade.

Atomic force microscopy (AFM) images of the membrane surface were obtained under a Dimension V microscope (Veeco) (CNPEM-Campinas/SP). The images were obtained in *tapping mode* at 1 Hz, using silicon needles with a curvature radius of 15 nm and an inclination of 12°.

The membranes were analyzed by thermogravimetry in a TGA Instruments equipment, model Q500. The samples were heated to a heating ratio of 10 ºC/min in the range of 25 ºC to 900 ºC, under the nitrogen gas flow of 20 mL $^{min-1}$. The thermal degradation start-up temperatures (T_{onset}) were determined by the analysis of the thermogravimetric (TG) and derived thermogravimetric (DTG) curves. The onset T was calculated by the intersection of the extrapolation line from the beginning of the thermal event with the tangent to the curve at the temperature of the maximum rate of thermal degradation of the material (observed in the DTG curve).

The differential exploratory calorimetry (CSD) measurements of the membranes were performed in a TA Instruments equipment, model DSC Q-100. The tests were performed in nitrogen atmosphere under a heating rate of 20 ºC $^{min-1\ in}$ the range of -50 ºC to 300 ºC.

For the dynamic-mechanical thermal analysis (DMTA) assay, the membranes were cut with the aid of a mold and a scalpel with stainless steel blade for the manufacture of rectangular specimens (5 x 30 mm^2). The tests were performed on a DMA Q800 equipment from TA Instruments operating in traction mode at 1 Hz and with a amplitude of 0.005 mm. The temperature was varied from -30 to 180 °C with a constant heating rate of 2 °C min^{-1}.

In the same equipment and with the same standard of specimens, mechanical tests were performed under traction to obtain stress curves – strain according to ASTM D882-18 standard with modifications [39]. The test was performed at room temperature and test speed of 1 N min-1. From the curves σ – ε the values of maximum stress (MPa), deformation at rupture (%) and elastic modulus (MPa) were determined. For these assays, at least 6 specimens of each sample were tested.

To analyze the water absorption capacity, the moistened and dried masses of the membranes were obtained on an analytical scale. The water absorption capacity of the membranes (ΔM) was calculated from equation (16):(16)1

$$\Delta M = \frac{M_u - M_S}{M_S} \qquad (16)1$$

where M_u is the moist membrane mass and $M_{s\ is}$ the dry mass. Dry mass (M_s) was obtained after heat treatment of the sample in an oven at 60 ºC for 24h. To measure the wet mass (M_u) the membranes were kept in deionized water at 80 ºC for 1h. Before the mass check, the excess water from the membrane surface was carefully removed with filter paper.

The proton conductivity (σ) of the membranes was determined by Electrochemical Impedance Spectroscopy (EIE) using a Solartron 1260 frequency analyzer and a teflon sample port equipped with two electrical connection terminals. Measurements were performed at room temperature with dry and wet samples.

For this analysis, an ac excitation of 200 mV was used in the frequency range of 30 MHz to 10 MHz, with ten points per decade of frequency.

The resulting Nyquist diagrams were treated using Zahner's THALES software to determine the values of the resistances of the samples (R). Conductivity (σ) was calculated using Equation (17), using membrane thickness L (cm), Resistance of Membrane R (Ω) and cross-sectional area of membrane A (cm(17)2^2) [27].

$$\sigma = \frac{L}{R.A} \qquad (17)2$$

Preparation of catalyst coated membranes (CCM)

The manufactured membranes and the commercial Nafion membrane were used for testing in an electrolytic cell with proton exchange membrane (PEMEC). To perform these tests, catalyst-coated membranes (MCC) were manufactured. The MCC is composed of an electrolyte (membrane) positioned between two electrodes (anode and cato).

The CCMs with an active area of 3.98^{cm2} were prepared using the Decal method (also called the transfer method) where the electrodes (catoand anode) are initially deposited on inert teflon substrates and then transferred to the membrane by $^{\text{hot pressing 40}}$.

Initially for the preparation of the electrodes, paints containing catalyst powder, 10% Nafion solution (m/m) were produced in water (D1021, DuPont) and organic alcohol. The catalyst powders used in the production of anodic and cathode electrodes were IrO_2 (Alfa Aesar, Premion, 99.99%) and 60% Pt/C (HiSPEC 9100, Johnson & Matthey), respectively.

The inks were dispersed in an ultrasonic homogenizer (Bandelin Sonopuls HD 3200) and deposited on inert teflon substrates with the aid of a dosing blade (Coatmaster 509 MCI, Erichsen GmbH & Co. KG). The electrodes were dried in a resistive oven at 60°C for 3h. Finally, the dry electrodes were positioned one on each side of the membranes and hot pressed at 100 ºC under pressure of 200 kgf $^{cm-2}$ for 3min. The catalytic layers of the anode and the orpt obtained final loads of 2.1 mg Ir cm-2 and 0.8 mg Pt cm-2, respectively.

Electrolytic cell test with proton-changing membrane (PEMEC)

The membranes coated with catalyst (CCMs) manufactured were tested in an electrolytic cell with proton exchange membrane (PEMEC) to obtain polarization curves. The tests were performed using a Greenlight E60 test station. The porous transport layers (PTLs) used in the box

and anode were manufactured from titanium plates (Bekaert) with 68% porosity and 350 μm thickness of Bekaert. The anodic and cathode PTLs were coated with iridium creating superficial layers 0.5 mg cm^{-2}.

To perform the tests each CCM was positioned between the PTL and then the set was placed inside the electrolyte cell. The cell was then compressed using a press and then positioned at the test station where all inputs and outputs were connected.

The start of the test occurred with the heating of the electrolytic cell up to 80 °C. Ultrapure water was preheated to the same cell temperature and supplied at a flow rate of 50 mL $^{min-1}$ to the anode compartment. Before the beginning of the generation of the polarization curve, the electrolytic cell was preconditioned the current densities of 0.2 and 1 A $^{cm-2}$ for 1h. After this step, the polarization curve was made by applying predetermined current values, each current applied was maintained for 5min for the verification of the voltage obtained. The current has been increased to a maximum of 2.0 V. The results presented are the result of an average of at least three polarization curves.

RESULTS AND DISCUSSION

In order to verify the effect of the incorporation of the different nanocellulose nanocrystals in the Nafion matrix, a characterization was performed in terms of composition, structure, morphology, thermal and viscoelastic properties and prosthetic conductivity. In addition, the membranes were tested in an electrolytic cell with proton-changing membrane.

The analysis of Nafion and its nanocomposites by means of vibrational spectra in the infrared region provides information on the chemical and morphological characteristics of the obtained material. Commercial Nafion (Nafion 115), Conformation Nafion (Ncast) and

nanocomposites with the addition of commercial cellulose nanocrystals (N/CNC_C) and obtained by enzymatic hydrolysis of sugarcane straw (N/CNC_ENZ) were analyzed using the FT-IR technique and the spectra obtained are presented in Figure 1.

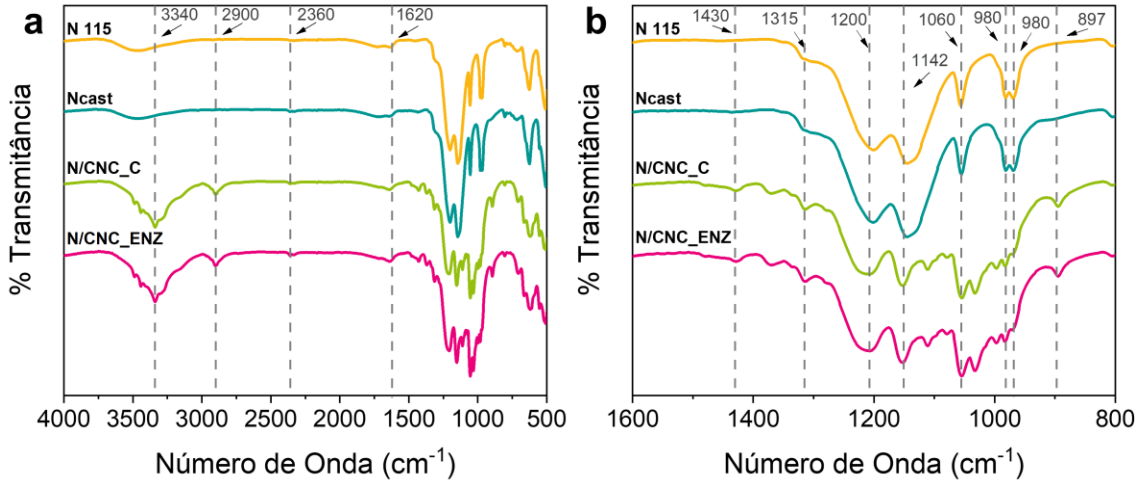

Figure 1 – (a) Fourier transform infrared spectroscopy spectra (FTIR) for commercial Nafion membrane (N115), Nafion obtained by casting (Ncast), Nafion nanocomposite with commercial CNCs (N/CNC_C) and Nafion nanocomposite with CNCs obtained by enzymatic hydrolysis of sugarcane straw (N/CNC_ENZ); (b) magnifications of the same spectra in the spectral range from 1600 to 800 cm-1.

All analyzed samples showed the main characteristic bands of Nafion, the positions in the spectrum of these energy absorption bands in the infrared region are found in Table 1. The maintenance of these bands in the samples produced by the forming process is indicative that the method adopted did not affect the integrity of the polymer chains, branches and sulphonic groups, responsible for the morphology, mechanical and electrical properties of the polymer.

Table 1 - Main absorption bands characteristic of Nafion [28.41]

Band position (cm^{-1})	Connection	Denomination
2360	**-CF 2-CF_2-**	**Stretch**
1620	**OH**	**Angular deformation**
1200	**CF_2 and SO_3^-**	**Asymmetric stretch**
1142	**CF_2 and SO_3^-**	**Symmetrical stretch**
1060	**-SO_3^-**	**Symmetrical stretch**
980	**-C-O-C-**	**Stretch**
960	**-C-O-C-**	**Symmetrical stretch**

The band observed at 2360 cm^{-1} is associated with the main polishing chain formed by -CF 2-CF 2-bonds. The band at 1620 cm^{-1} is generated by the presence of water contained in the polymer structure. The bands observed at 1200, 1142 and 1060 cm^{-1} may indicate the existence of sulphonic groups on the membrane, and represented respectively the asymmetric stretch vibration of the S=O bond, the symmetrical stretch vibration of the S=O lead and the symmetrical S=O stretch. can also be attributed to the asymmetric and symmetrical stretch of the C-F bond present in the main chain of the Nafion. The bands at 980 and 960 cm^{-1} present the typical absorbance of the C-O-C bond present in the lateral chains of Nafion [30,41].

In addition to the verification of the characteristic bands of Nafion, the FTIR spectra of the obtained materials were also analyzed to verify the presence of residual solvents of the forming process. The solvent used in the conformation process was DMSO, when the incomplete removal of this solvent from the polymer matrix occurs, the spectra of the samples can present three characteristic bands of this solvent in 2657, 1659, and 1410 cm^{-1}. The bands at 2657 and 1410 cm^{-1}

are associated with the C-H binding of the methyl group present in the DMSO. The band at 1659 $^{cm-1}$ is assigned the C=O and S=O bonds of the solvent [36]. In the spectra of the membranes produced, none of the characteristic bands of DMSO were observed, suggesting that there is no solvent residue in the manufactured membranes.

Regarding the spectra of the nanocomposites, the observed patterns are consistent with the expected chemical structure and composition due to the presence beyond the characteristic bands of Nafion also of the absorption bands of cellulose nanocrystals (Table 4.2). The main bands observed that evidence the maintenance of CNCs in the matrix are 3340 cm^{-1} (stretch O-H), 2900 $^{cm-1}$ (stretch C-H), 1430 $^{cm-1}$ (asymmetric deformation C-H and C-O), 1315 $^{cm-1}$ (c-h angular symmetric deformation), 897 $^{cm-1}$ (c-o-c and c-h stretch). The characteristic band of cellulose at 1061 $^{cm-1}$ referring to the stretching of groups C-O and C-H cannot be identified, because it may overlap the symmetrical stretch band of the sulphonic group present in the Nafion.

The effect of the introduction of cellulose nanocrystals in the polymermatrix of Nafion in relation to the crystallinity of the membrane obtained was evaluated by X-ray diffraction. According to difratograms presented in Figure 2, the X-ray pattern of pure Nafion membranes (N115 and Ncast) are similar and characteristic of a semicrystalline material with a wide diffraction peak at 2θ between 12 º and 20 º. This observed peak is the result of the overlap of a crystalline peak (2θ = 17.5º) and an amorphic halo (2θ = 16º) of the perfluoroeter lateral chains of Nafion[36,42].

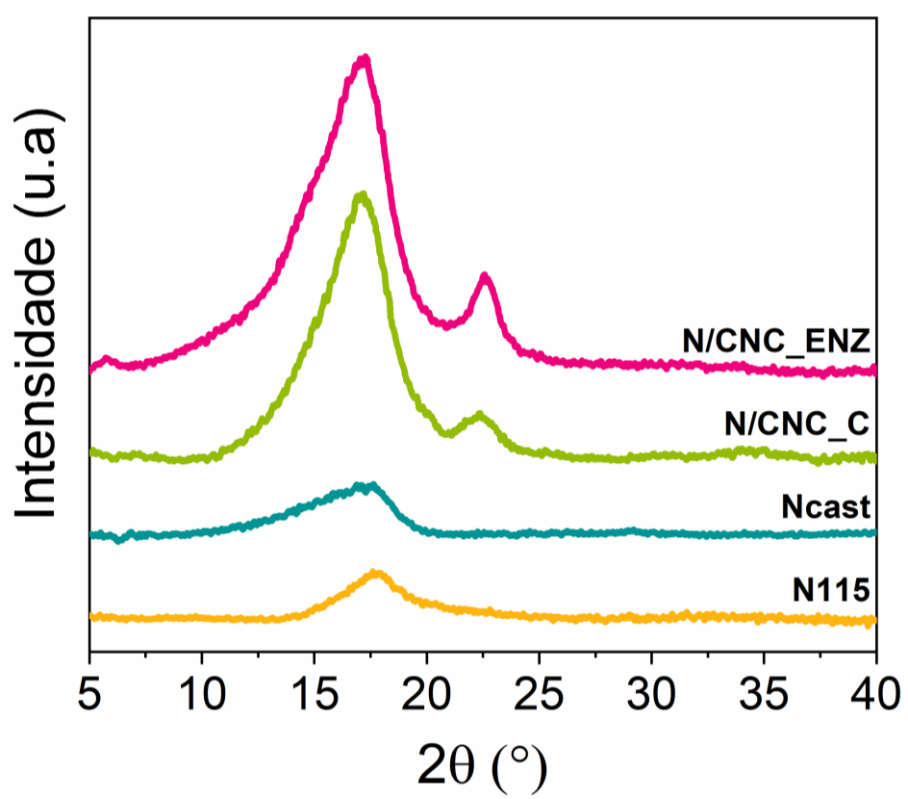

Figure 2 X-ray diphrates for commercial Nafion membrane (N115), Nafion obtained by casting (Ncast), Nafion nanocomposite with commercial CNCs (N/CNC_C) and Nafion nanocomposite with CNCs obtained by enzymatic hydrolysis of sugarcane straw (N/CNC_ENZ).

As expected, the diffraction pattern of nanocomposite membranes (N/CNC_C and N/CNC_ENZ) corresponds to an overlap of the difratograms of the isolated components (Nafion and cellulose). In these materials it was possible to observe mainly the appearance of the peak in 2θ = 23° referring to the cellulose plan 002 [43–46]. There was also a considerable increase in the peak of broad diffraction at 2θ between 12 º and 20 º probably caused by the overlap of the characteristic peaks of the Nafion with the peaks of cellulose at 2θ equal to 15 ° (plane 101), 17 ° (plane 10) $\bar{1}$[43–46].

Finally, the appearance of crystalline peaks characteristic of cellulose in the difratograms of the nanocomposite membranes produced can be considered evidence that the embedded cellulose nanocrystals did not suffer degradation during the acquisition of membranes.

To evaluate the changes in the morphology of the Nafion matrix caused by the incorporation of the different nanostructures, the samples were analyzed by atomic force microscopy (AFM), as can be observed in Figure 3. The observed surfaces for the commercial Nafion samples (Figure 3a) and for the Nafion obtained by the solvent evaporation process (Figure 3b) have a rough surface characteristic of Nafion, formed by aggregates in the form of nanometric particles approximately cylindrical.

In order to evaluate the distribution of cellulose nanocrystals along the polymer matrix, AFM images were obtained from both sides of the samples (top and bottom). In both samples containing commercial and enzymatic CNCs, there was a homogeneous distribution of nanoparticles, and a similar number of nanoparticles can be observed both at the top and bottom of the membranes.

Regarding the dispersion of the nanoparticles, it was evident that the membranes prepared from the commercial CNC presented more homogeneous dispersion when compared to membranes with enzymatic CNC. The probable cause of the variation in dispersion is due to the difference in loads on the surface of the nanostructures due to the different methods of obtaining. Commercial cellulose nanocrystals are produced through acid hydrolysis using sulfuric acid, a process that generates charged nanoparticles, which facilitates the dispersion process [44]. According to reports in the literature, suspensions of the commercial CNC (Maine) present high zeta potential values ~70 mV, being considered highly stable suspensions [48,49]. On the other hand, CNCs

obtained by enzymatic hydrolysis are nanostructures with lower amounts of loads and can be considered moderately stable (zeta potential between ~25 and 31 mV).

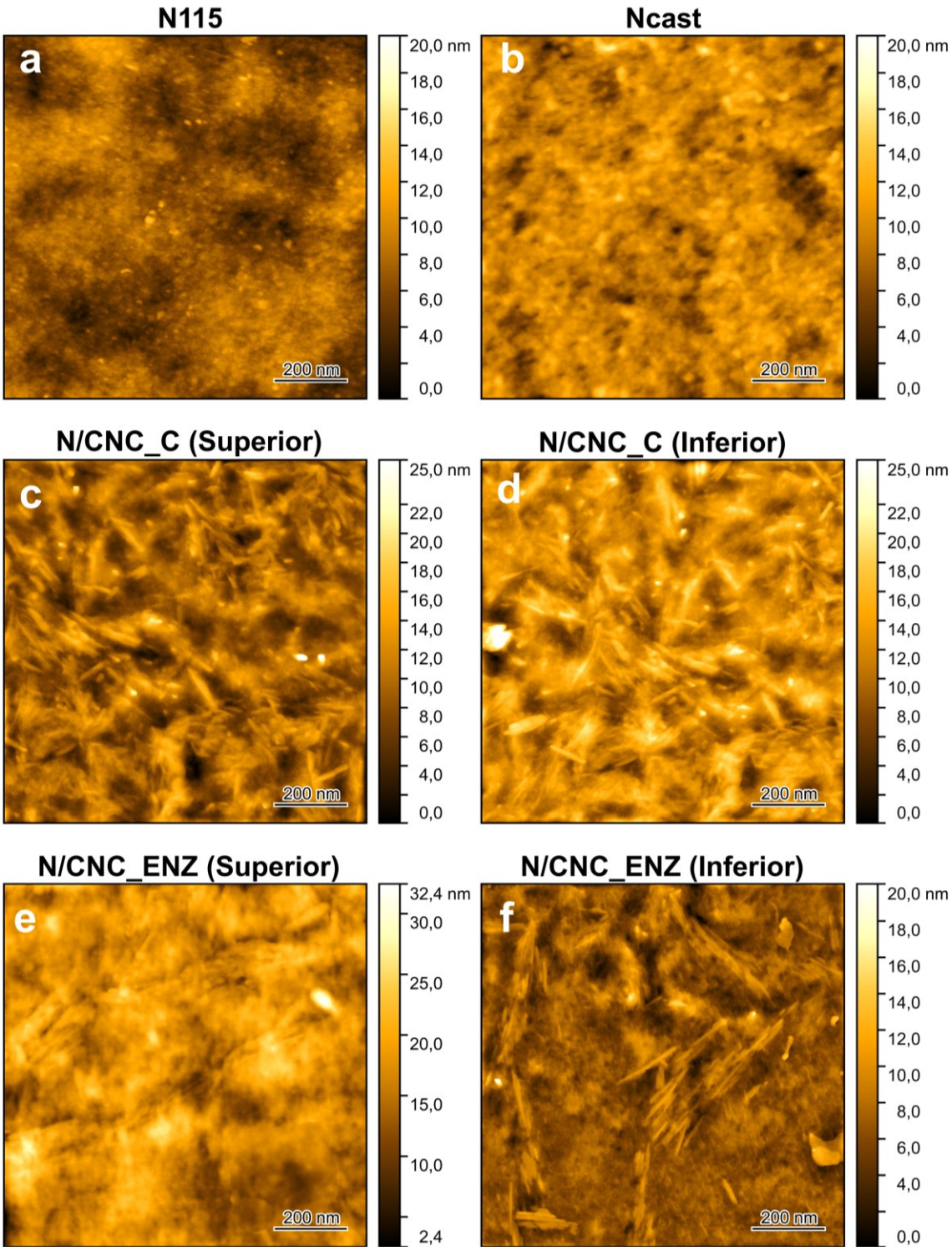

Figure 3 - Images obtained by atomic force microscopy (AFM) from the surface of (a) commercial Nafion membrane (N115), (b) Nafion obtained by casting (Ncast), (c-d) nano Nafion composite with commercial CNC (N/CNC_C) and (e-f) Nafion nanocomposite with CNC obtained by enzymatic hydrolysis of sugarcane straw (N/CNC_ENZ).

The thermal stability of Nafion membranes with and without cellulose nanocrystals was investigated using thermogravimetric analysis and the results can be observed in Figure 4 and Table 2.

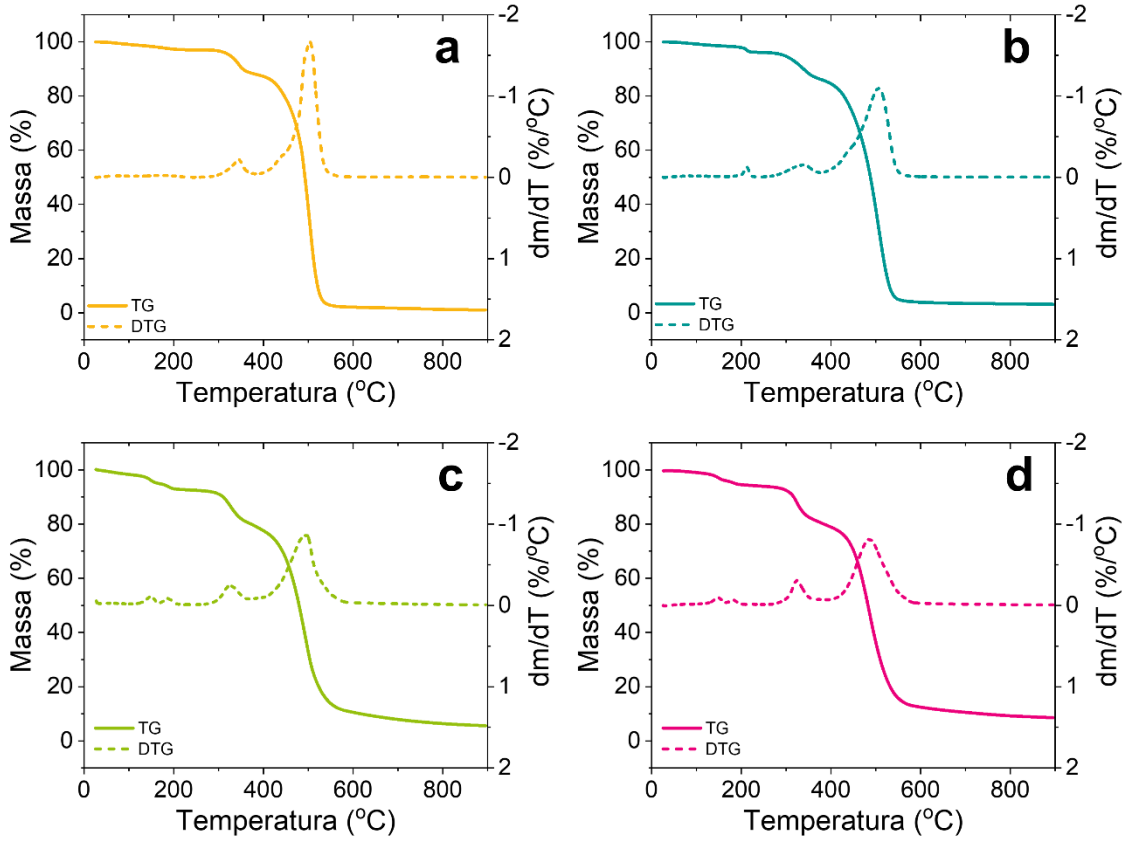

Figure 4 - TG/DTG thermogravimetry curves for (a) commercial Nafion membrane (N115), (b) Nafion obtained by casting (Ncast), (c) Nafion nanocomposite with commercial CNC (N/CNC_C)

and (d) Nafion nanocomposite with CNC obtained by enzymatic hydrolysis of sugarcane straw (N/CNC_ENZ).

Table 2 - Data obtained by TG/DTG for commercial Nafion samples (N115), Nafion obtained by casting (Ncast), Nafion nanocomposite with commercial CNC (N/CNC_C) and Nafion nanocomposite with CNC obtained by enzymatic hydrolysis of sugarcane straw straw (N/CNC_ENZ).

Sample	Temperature range (°C)	T_{onset} (°C)	T_{max} (°C)	Mass Loss (%)	Stable residue at 900 °C (%)
N115	25 to 230	150,3	172,0	2,87	1,17
	230 to 370	321,5	344,7	8,49	
	370 to 600	471,5	503,9	86,49	
Ncast	25 to 230	204,8	210,8	3,79	0,65
	230 to 370	300,0	338,2	9,60	
	370 to 600	460,8	505,8	82,66	
N/CNC_C	25 to 170	135,0	149,8	5,55	3,04
	170 to 230	178,8	188,07	2,28	
	230 to 370	304,0	324,9	12,49	
	370 to 600	452,9	496,5	69,62	
N/CNC_ENZ	25 to 170	134,7	148,8	3,93	5,34
	170 to 230	174,0	183,0	1,74	
	230 to 370	306,1	323,7	13,20	
	370 to 600	451,1	485,0	68,55	

As can be seen in Table 4.7 (a) both commercial Nafion and Nafion produced by casting presented three mass loss events typical of this type of material. The first event of mass loss is due to moisture evaporation and extends to approximately 230 °C, between 230 and 370 °C occurs the second event attributed to the degradation of the sulphonic groups present in the side chains [50], since the mass loss observed between 370 and 600 °C is associated with degradation of the main chain of Nafion [50].

In relation to the membranes produced with cellulose nanocrystals Table 4.7 (c-d) the thermal degradation profile was similar for the two samples. Through the analysis of the DTG graphs of these samples it is possible to observe four thermal events with maximum decomposition temperatures at approximately 150, 185, 325 and 490 °C. In addition to moisture loss, thermal events that have the highest maximum decomposition temperatures (325 and 490 °C) occur in the same interval as the events observed for Nafion, suggesting the same origin. On the other hand, the events observed with maximum decomposition temperatures at approximately 185 °C may originate due to the degradation of the cellulose nanocrystals contained in the samples. Although the CNCs both commercial and those produced by enzymatic hydrolysis present thermal degradation onset temperatures above 200 °C[51] and 300 °C, respectively, there are studies that point to a compromise of the thermal stability of cellulose when used for the production of nanocomposites [28,30]. According to Noonan et [al. 29] the sulphonic groups present in Nafion are capable of generating a catalytic effect that facilitates the thermal degradation of the hydroxyl groups that make up cellulose.

Although the membranes with CNCs present thermal decomposition onset temperatures below those observed for pure Nafion membranes, the nanocomposites produced presented

sufficient stability to be used in electrolytic cells with proton-changing membrane since the operating temperature of these equipments is less than 100 °C.

Differential exploratory calorimetry (CSD) analysis was used to investigate the thermal behavior of pure Nafion membranes with CNCs. Figure 5 presents the DSC curves of the first heating for polymer membranes.

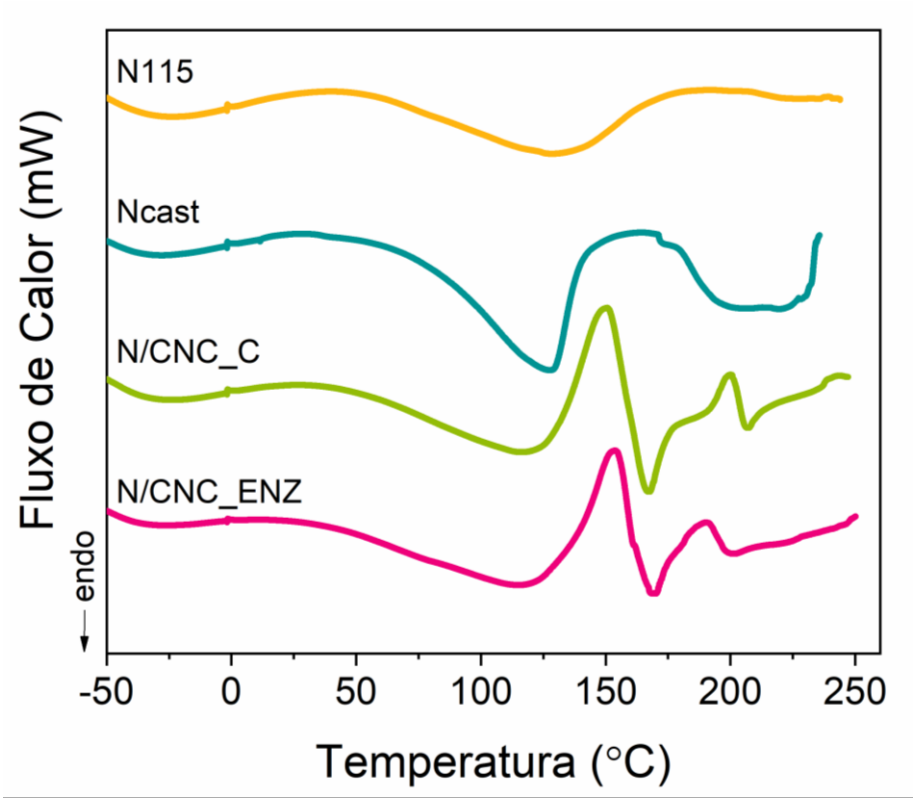

Figure 5 – Differential scanning calorimetry curves of commercial Nafion membranes (N115), Nafion obtained by casting (Ncast), Nafion nanocomposite with commercial CNC (N/CNC_C) and Nafion nanocomposite with CNC obtained by enzymatic hydrolysis of sugarcane straw (N/CNC_ENZ).

The CSD curve obtained for commercial Nafion presented two endothermic peaks, one at approximately 130 ºC and the other with a wider characteristic at approximately 230 ºC, results

that agree with what has already been reported in the literature [for this material 52,53]. The first peak at approximately 130 ºC can be attributed to the glass transition temperature (*Tg*) of the sulfion [groups 53] and the second peak, around 230 ºC, to the fusion of the crystalline [regions 53].

The DSC curve of the Nafion membrane obtained by casting also presented the two most endothermic peaks characteristic of Nafion. *Tg for* this material showed a slight reduction of approximately 5 ºC when compared to commercial Nafion. This reduction in *Nafion Tg* obtained by casting when compared to the commercial has already been reported in the literature [50]. According to Matos et [al. 50] Nafion membranes obtained by casting may present a lower crystallinity when compared to the commercial membrane produced by extrusion. This reduction in crystallineness facilitates the mobility of polymer chains thus reducing the glass transition temperature.

In membranes with CNCs, the addition of both types of nanoparticles caused an overlap of thermal events that can be related both to the fusion of the Nafion matrix and to the thermal degradation of the CNCs, as already observed in the TGA analysis (Figure 4).

Dynamic-mechanical thermal analysis (DMTA) was performed to evaluate the viscoelastic properties of membranes produced with and without CNCs, the results can be observed in Figure 6.

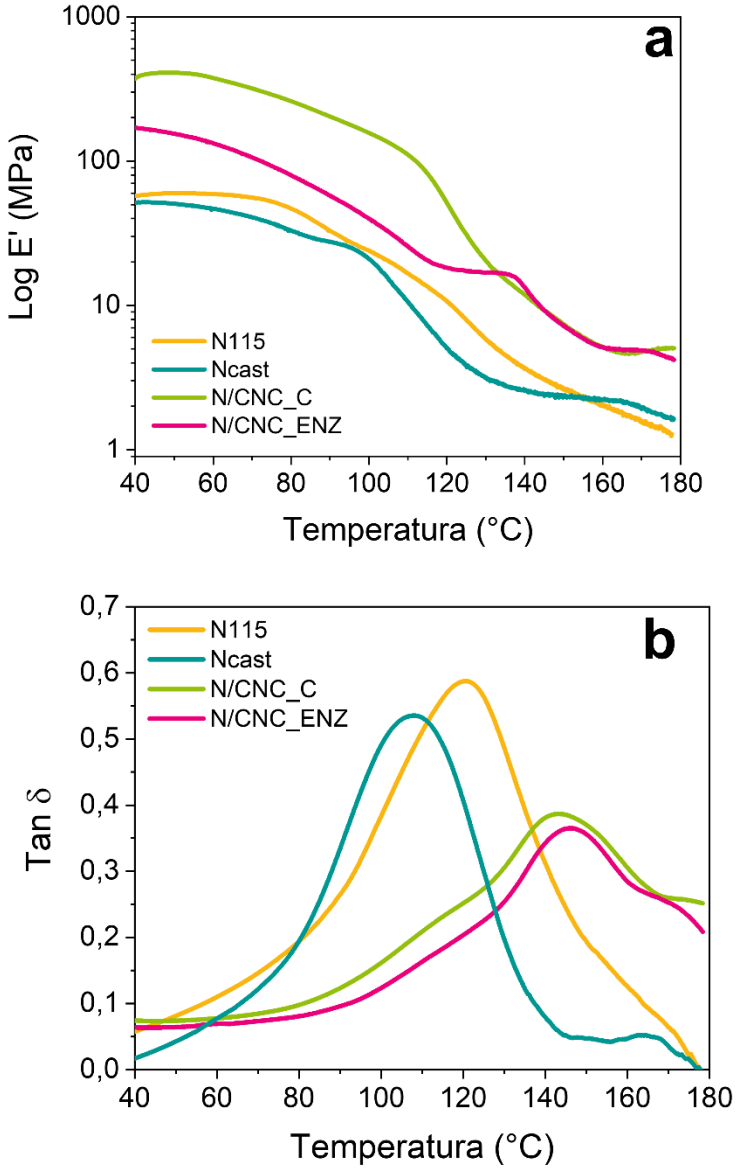

Figure 6 – Dynamic-mechanical thermal analysis (a) storage module and (b) damping factor as a function of the temperature of the membranes of commercial Nafion (N115), Nafion obtained by casting (Ncast), Nafion nanocomposite with commercial CNC (N/CNC_C) and Nafion nanocomposite with CNC obtained by enzymatic hydrolysis of sugarcane straw (N/CNC_ENZ).

For the commercial Nafion membrane the storage module (E') decreases with the temperature increase and between ~90 and ~140 ºC this reduction of E' becomes more pronounced.

The associated transition presents a maximum in the tanδ curve at ~120ºC and represents the vitreous transition of material [54].

The Nafion membrane produced by conformation presented a viscoelastic behavior similar to the commercial membrane. For this material, the tanδ curve presented a maximum of approximately 110 ºC, evidencing a *reduction in the Tg* of the material when compared to the commercial membrane, a result that agrees with what was already observed through the results of the CSD analysis.

The storage module for membranes produced with CNC was superior to that observed for pure membranes throughout the temperature range analyzed. This result confirms the role of CNCs in reducing membrane deformation during heating. Moreover, the increase in the storage module was more evident for the membrane produced with commercial CNC, this difference is probably due to the greater dispersion of cncs in the Nafion matrix, as already observed through the Analysis of AFM (Figure 3). In the tanδ curve it is possible to observe an overlap of peaks between ~80 and ~180 ºC, this overlap of events can be correlated both the vitreous transition of the Nafion and the process of mass loss already observed for the same temperature range through thermogravimetric analysis (Figure 4). In addition, this displacement from peak to higher temperatures may be related to the restriction of movement of Nafion chains caused by the insertion of CNCs, a factor that also generates an increase in the glass transition temperature of the material.

Mechanical properties of the samples were investigated by tensile tests. The stress-strain curves that best represent the behavior of the materials are illustrated in Figure 7, and the results calculated by analyzing the replicate assays of each material are presented in Table 3.

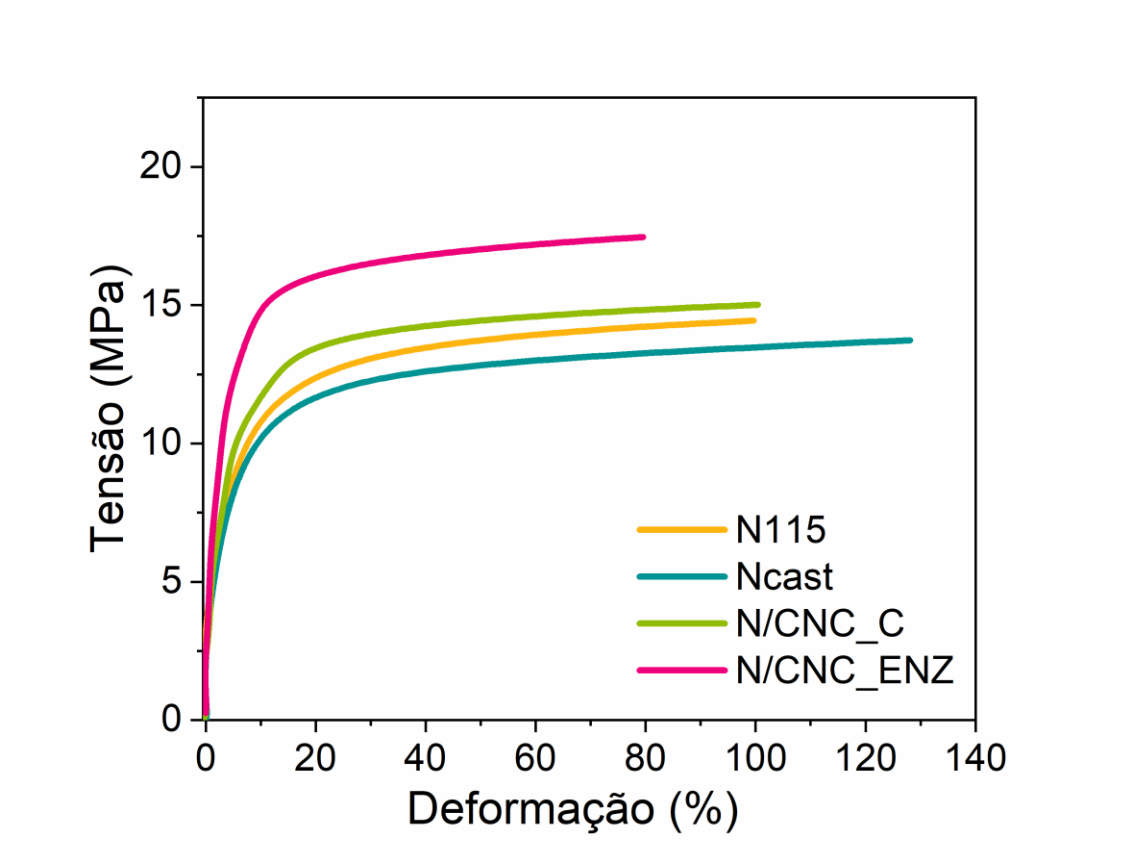

Figure 7 - Representative stress curves as a function of the deformation of membranes with and without cellulose nanocrystals.

Table 3 - Mechanical engineering properties of membranes with and without cellulose nanocrystals.

Sample	Mechanical properties		
	Elastic module (MPa)	Maximum voltage (MPa)	Deformation (%)
N115	245.6 ± 8.5	14.3 ± 0.5	100.4 ± 9.0
Ncast	149.3 ± 4.9	13.9 ± 0.3	124.3 ± 8.8
N/CNC_C	272.9 ± 8.1	15.9 ± 0.8	98.3 ±
N/CNC_ENZ	403.3 ± 9.0	16.5 ± 0.7	78.9 ± 5.0

From the stress-strain curves (Figure 7) it is possible to notice that the Nafion obtained by casting presented a more dubious behavior, represented by the higher level of deformation, while commercial Nafion presented a slightly more fragile behavior, represented by higher mechanical resistance. The incorporation of CNCs in the Nafion matrix caused a decrease in the level of deformation and an associated stress gain, thus altering the mechanical behavior of the polymer.

These results corroborate those already reported in the studies of Noonan and collaborators [29]. The authors also used cellulose nanoparticles (nanofibrils) to produce Nafion matrix nanocomposites from solvent evaporation conformation. The result of this study also demonstrated that the incorporation of this type of nanoparticle in the Nafion generates an increase in the maximum stress, but a lower deformation of the material.

The mean values of the elastic modulus, maximum stress and strain for nafion samples with and without CNC are presented in Table 4.8. These results show that the sample prepared with enzymatic CNC presented the largest elastic modulus. However, in this sample, the lowest deformation in rupture was also observed. This result may be associated with the formation of clusters, as already observed by AFM images (Figure 3). The clusters of CNCs acted as stress concentration points that accelerated the failure and resulted in lower tensile strength of the nanocomposites

The hydration capacity of membranes is another important parameter to be investigated, because it influences the proton conductivity of the membrane, an essential factor for its application in electrolytic cells with proton-changing membrane (PEMECs). The prosthetic conductivity of the membrane can be increased by increasing humidification [56]. Water absorption capacity was measured for all membranes studied and the results are presented in Table 4.

Table 4 - Water absorption capacity in the membranes of commercial Nafion (N115), Nafion obtained by casting (Ncast), Nafion nanocomposite with commercial CNC (N/CNC_C) and Nafion nanocomposite with CNC obtained by enzymatic hydrolysis of sugarcane straw (N/CNC_ENZ).

Sample	Water absorption (% by mass)
N115	**35.5 ± 0.5**
Ncast	**47.7 ± 0.5**
N/CNC_C	**54.6 ± 0.1**
N/CNC_ENZ	**58.2 ± 0.1**

The experimental data regarding the water absorption capacity observed for the commercial membrane Nafion 115 are similar to those found in articles and manufacturer specifications [50.57]. On the other, the water absorption capacity of the membrane obtained by casting was higher than that observed for the commercial membrane. This variation in humidification capacity may be associated with the difference in crystallineness of the members. The crystalline regions limit the expansion of polymer chains and ensure the mechanical stability of the material. Thus, for the sulphonic group to expand and absorb water, the expansion must overcome the elastic energy of the polymer chains, and this energy is greater when the material has greater crystallineity [58]. The membrane obtained by conformation presents a lower crystalline ity when compared to the commercial one obtained by an extrusion process. Thus, a lower

crystalline of the chain gives the polymer a lower resistance to its expansion, a factor that increases the membrane's water absorption capacity.

The insertion of CNCs (commercial or enzymatic) in the Nafion matrix conferred the membranes a significant increase in humidification capacity when compared with the 100% Nafion membrane also obtained by conformation. This behavior can be explained by the presence of hydroxyl groups on the surface of cellulose nanocrystals, which guarantees this material a high water absorption capacity [59]. Furthermore, a more evident increase in water absorption capacity can be observed for membranes produced with enzymatic CNC. This increase in this property may be due to the process of obtaining the nanocrystals. With the above, the enzymatic CNC, unlike the commercial CNC, is produced through hydrolysis without the use of strong acids, such as sulfuric acid, which promotes the extraction of nanoparticles with a surface predominantly composed of hydroxyls [60].

In the literature there are reports of increased water absorption capacity with the incorporation of nanocellulose in Nafion matrices [30,56]. In the work of Jiang et al. [30], where Nafion membranes were produced through the solvent evaporation conformation technique, an increase in the ability to absorb water was observed with the incorporation of nanocellulose into the Nafion matrix (between 10 and 50% (m/m)).

The analysis of the electrical conductivity (ionic) of the samples was performed by means of impedance spectroscopy measurements using the dry and moistened membranes. Figure 8 shows impedance spectroscopy diagrams for (a) wet and (b) dried samples. From the experimental data, it was possible to determine the conductivity of the membranes, the values obtained are presented in Table 5.

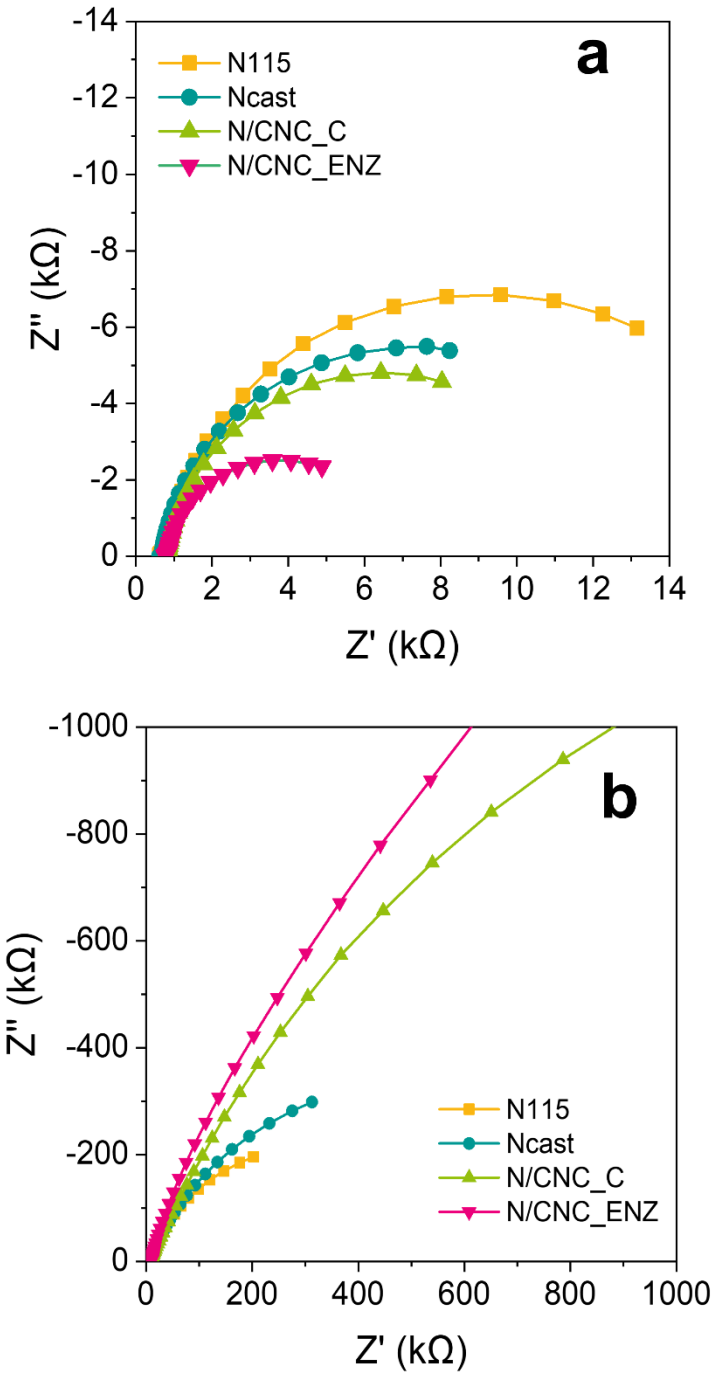

Figure 8 - Nyquist graphs obtained by electrochemical impedance spectroscopy at 200 mV obtained from wet and (b) dry membranes.

Table 5 - Estimated protein conductivity from nyquist graphs of wet and dry membranes.

Sample	Conductivity σ ($^{mS.cm-1}$)
N115 (dry)	0,7
Ncast (dry)	0,4
N/CNC_C (dry)	0,2
N/CNC_ENZ (dry)	0,1
N115 (wet)	27,1
Ncast (wet)	28,0
N/CNC_C (wet)	33,7
N/CNC_ENZ (wet)	47,3

With dry membranes it is possible to observe that the added CNCs led to the reduction of the conductivity of the membranes. Nanocelluloses (such as CNCs and CNFs) at low humidity present very low conductivity (~ 1x10-4 $^{mS.cm-1}$), especially when compared to the conductivity of Nafion [27]. Thus, CNCs added to Nafion at low humidity can be considered isolated. Thus, causing a reduction of the electrical conductivity of the electrolyte by the volumetric fraction occupied by isolated particles.

The objective of this work is to use the membranes produced as proton exchange membranes in water electrolysis cells. During the electrolysis process, the membranes are kept in contact with water, so it is important to analyze their behavior in the wet state. By comparing the tests performed with the wet and dry membranes it was possible to observe that the conductivity

of all samples is increased with the enposition of the material. This is a typical behavior for proton-conducting polymers such as Nafion, where water acts as a means for transporting loads [27].

The conductivity values obtained for wet commercial Nafion are in accordance with the values reported for this polymeric electrolyte under similar conditions [27]. The wet Ncast membrane presented conductivity superior to that of commercial Nafion. This difference can be explained by the fact that Ncast has a higher water absorption capacity. The greater humidification of the membranes produced by conformation decreases the average free path for the conduction of the protonic conduction, thus increasing the conductivity of the material [58].

The data presented in Table 5 show that the conductivity of wet samples increases with the addition of CNCs. For nanocomposites formed from the addition of commercial CNC this increase is ~ 6 $mS.cm^{-1}$. The nanocomposites formed with enzymatic CNC this increase is even more evident reaching an increase of ~ 20 $mS.cm^{-1}$. This more expressive increase for samples produced in zymatic CNC may be caused by the greater capacity to absorb water from these membranes, as can be observed in Table 4.9.

An increase in the conductivity of Nafion by the insertion of cellulose nanocrystals was also reported in the work of Hasani-Sadrabadi and 31 collaborators. In this study, Nafion membranes with 5% (m/m) of CNC were produced through the conformation technique and an increase in proton conductivity was observed in the entire temperature range between 25 and 120 ºC. According to the authors, the CNCs act by connecting the hydrophilic domains of The Nafion (Closters), thus increasing the number of channels available for proton transport.

The membranes produced and the commercial membrane were tested in an electrolytic cell with proton exchange membrane (PEMEC). To perform the tests at least three samples of each membrane were coated with standardized loads: 2.1 mg cm^{-2} of iridium on the anodyne side and 0.8

mg $^{cm-2\ of}$ platinum on the cathode side. The tests were performed on all samples using the same parameters. Figure 9 shows the current *versus* voltage profiles (polarization curves) obtained during the tests of the membranes in electrolytic cell. The values of the potentials (V) presented by the electrolyte cell during the application of certain current densities in each membrane can be observed in Table 6.

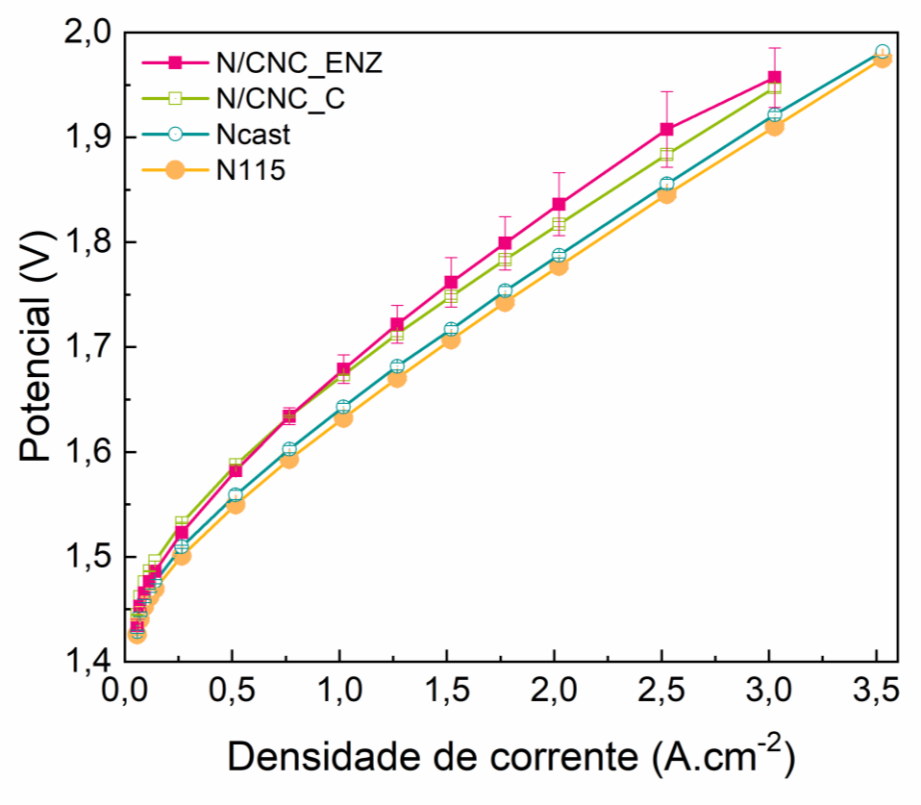

Figure 9 - Polarization curve of the electrolytic cell with proton-changing membrane.

Table 6 - Potentials presented by the electrolyte cell during the application of different current densities.

Membrane	Cell potential at 1 $A \cdot cm^{-2}$ (V)	Cell potential at 2 2 $A \cdot cm^{-2}$ (V)

N115	1.63 ± 0.00	1.78 ± 0.00
Ncast	1.64 ± 0.00	1.79 ± 0.00
N/CNC_C	1.67 ± 0.00	1.81 ± 0.00
N/CNC_ENZ	1.68 ± 0.01	1.84 ± 0.03

The polarization curves presented for all samples present the two typical regions of polarization curves of a PEM electrolysis. At low current densities, the cell's potential rises sharply as a result of activation polarization. At higher current densities, the cell potential rises linearly with the current as a result of ohmic fall (cell resistance) [40].

The membranes produced by conformation containing 100% Nafion showed a slight decrease in performance when compared to that of commercial Nafion. As can be seen in Table 6, with the application of a current density of 1 $A \cdot cm^{-2}$, a performance fall of ~ 10mV was verified. The same performance fall was also verified for higher current densities.

A reduction in performance was observed for cnc-containing membranes. For the membrane with commercial CNC during the application of a current density of 1 $A\ cm^{-2}$, a performance fall of ~ 40mV was observed in relation to the commercial membrane. The membrane containing enzymatic CNC also promoted a performance fall when compared to the commercial membrane. However, due to the greater deviations observed among the replicates of the tests of these samples, it is not possible to affirm that the membrane with enzymatic CNC has a performance different from that with commercial CNC.

According to the electrochemical impedance spectroscopy assays (Table 5) it was already possible to observe that the addition of CNCs in the Nafion matrix helps to increase the conductivity of the material, a fact that should contribute to the increase of membrane performance.

Thus, a possible explanation for the fall of remains of this material would be a lower addition of the catalytic layers (anode and cato) the membrane. As can be seen in AFM images (Figure 3), the membranes produced with CNC showed a higher roughness on both sides of the membranes. These reliefs on the surfaces of the membranes are able to decrease contact with the catalyst during its deposition reducing the connection between the parts.

Despite the slightly lower performance of cnc-containing membranes, the results observed here prove the possibility of application of these nanocomposite membranes in electrolytic cell with proton-changing membrane (PEMEC).

CONCLUSIONS

The results showed that CNCs can be effectively extracted from lignocellulosic biomasses of sugarcane (bagasse and straw), using the enzymatic route. These results revealed a more environmentally correct alternative route for the production of CNCs, which could be explored in order to add value to agroindustrial lignocellulosic biomass residues.

The yields and properties of CNCs varied according to the duration of hydrolysis reaction, indicating that this variable can be modulated to obtain a nanomaterial with greater crystallineity and more homogeneous size distribution. On the other hand, the thermal stability of the CNC suffered small variations with the enzymatic hydrolysis time, *presenting onset T values of* approximately 310 °C for the different samples. Therefore, the enzymatic hydrolysis conditions used resulted in nanocellulose with high crystalline and thermal stability, important parameters for the use of this material in various applications, including as reinforcement in nanocomposites.

Among the protocols for the production of CNC via enzymatic hydrolysis studied, the production route that was shown to be the most promising was the 72-hour duration in fibers

treated with sugarcane straw. This protocol showed a higher balance of properties in relation to aspect ratio, crystalline index and thermal stability.

Cnc-based nanocomposite membranes were produced, both enzymatic and commercial. The solvent evaporation forming technique adopted was able to produce CNC-containing membranes distributed throughout the material. However, due to the absence of loads in the enzymatic CNC, in this material it was possible to observe the formation of nanoparticle agglomerates.

Although the membranes with CNCs presented lower thermal stability when compared to those observed for pure Nafion membranes, the nanocomposites produced presented sufficient stability to be used in PEMEC, since the operating temperature of these equipments is less than 100 °C.

Through the DMTA technique it was possible to observe that both the conformation process caused a reduction in the glass transition temperature, however the results of the mechanical tests showed that the incorporation of CNCs in nafion generates an increase in the modulus and maximum stress, but a lower deformation of the material.

The insertion of CNCs in the Nafion matrix conferred the membranes a significant increase in humidification capacity when compared with the 100% Nafion membrane also obtained by conformation. In addition, an increase in the conductivity of the cntonic with the insertion of cncs was observed.

Despite the increase in conductivity, the performance of nanocomposite membranes when tested in a PEMEC was slightly lower than the commercial membranes. One reason for this result may be tied to the increased roughness of the surface of composite membranes. The lower

uniformity of the membrane surface may hinder the fixation of catalysts during the deposition process, which causes a performance to fall.

ACKNOWLEDGMENTS

The authors would like to thank the Brazilian research funding agencies FAPESP (grant #2016/10636-8), CNPq, SISNANO/MCTI, the Agronano Network, and the Brazilian Agricultural Research Corporation (Embrapa). To the German Scholarship Co-funded Research Grants – Short-Term Grants, Process 91752074. To Coordenação de Aperfeiçoamento de Pessoal de Nível Superior - Brasil (CAPES) for financial support to carry out this work with scholarship, process no. 88882.332728/2019-01. This study was financed in part by the Coordenação de Aperfeiçoamento de Pessoal de Nível Superior - Brasil (CAPES) - Finance Code 001.

REFERENCES

(1) Siqueira, G.; Fraschini, C.; Bras, J.; Dufresne, A.; Prud'Homme, R.; Laborie, M. P. Impact of the Nature and Shape of Cellulosic Nanoparticles on the Isothermal Crystallization Kinetics of Poly(-Caprolactone). *Eur. Polym. J. J.* **2011**, *47* (12), 2216–2227. https://doi.org/10.1016/j.eurpolymj.2011.09.014.

(2) Siqueira, G.; Abdillahi, H.; Bras, J.; Dufresne, A. High Reinforcing Capability Cellulose Nanocrystals from Extracted Syngonanthus Nitens (Golden Grass). *Cellulose* **2010**, *17* (2), 289–298. https://doi.org/10.1007/s10570-009-9384-z.

(3) Oliveira, F.B. de; Bras, J.; Pepper, M. T.B.; Curvelo, A.A. da S.; Belgacem, M. N. Production of Cellulose Nanocrystals from Sugarcane Bagasse Fibers and Pith. *Ind. Prod Crops.* **2016**, *93*, 48–57. https://doi.org/10.1016/j.indcrop.2016.04.064.

(4) FAOSTAT. *Top Production - Sugar Cane*. Food And Agriculture Organization Of The United Nations. http://www.fao.org/faostat/en/#home (accessed 2019-08-05).

(5) Camargo, L. A.; Pereira, S.C.; Correa, A.C.; Farinas, C.S.; Marconcini, J.M.; Mattoso, L. H.C. Feasibility of Manufacturing Cellulose Nanocrystals from the Solid Residues of Second-

Generation Ethanol Production from Sugarcane Bagasse. *Bioenergy Res.* **2016**, *9* (3), 894–906. https://doi.org/10.1007/s12155-016-9744-0.

(6) Bondancia, T. J.; From Aguiar, J.; Batista, G.; Cruz, A.J.G.; Marconcini, J.M.; Mattoso, L. H.C.; Farinas, C. S. Production of Nanocellulose Using Citric Acid in a Biorefinery Concept: Effect of the Hydrolysis Reaction Time and Techno-Economic Analysis. *Ind. Chem. Res.* **2020**, *59* (25), 11505–11516. https://doi.org/10.1021/acs.iecr.0c01359.

(7) Bondancia, T. J.; Batista, G.; Aguiar, J. De; Lorevice, V.V.; Cruz, A.J.G.; Marconcini, J.M.; Mattoso, L. H.C.; Farinas, C. S. Cellulose Nanocrystals from Sugar Cane Bagasse Using Organic and/ or Inorganic Acids: Techno-Economic Analysis and Life Cycle Assessment. **2022**. https://doi.org/10.1021/acssuschemeng.2c00061.

(8) Vanderfleet, O.M.; Cranston, E. D. Production Routes to Tailor The. *Nat. Rev. Mater.* https://doi.org/10.1038/s41578-020-00239-y.

(9) Squinca, P.; Bilatto, S.; Badino, A.C.; Farinas, C. S. Nanocellulose Production in Future Biore Fi Neries: An Integrated Approach Using Tailor-Made Enzymes. **2020**. https://doi.org/10.1021/acssuschemeng.9b06790.

(10) Ximenes, E.; Resources, R.; Carlos, S. Biomass into High-Value Products : Outcomes from a Long-Term. **2021**, 563–573. https://doi.org/10.1002/bbb.2179.

(11) Menander, L.M. S.; Cantarella, H.; Franco, H.C. J.; Kölln, O. T.; Pepper, M. T.B.; Sanches, G.M.; Rabelo, S.C.; Carvalho, J. L. N. Comprehensive Assessment of Sugarcane Straw: Implications for Biomass and Bioenergy Production. *Biofuels, Bioprod. Biorefining* **2017**, *11* (3), 488–504. https://doi.org/10.1002/bbb.1760.

(12) De Carvalho, D.M.; Colodette, J.L.; Perez, A.; García, J.C.; López, F.; Diaz, M. J. Ethanol-Soda Pulping of Sugarcane Bagasse and Straw. *Mr. Cellul. Chem. Technol.* **2014**, *48* (3–4), 355–364.

(13) El Miri, N.; Abdelouahdi, K.; Barakat, A.; Zahouily, M.; Fihri, A.; Solhy, A.; El Achaby, M. Bio-Nanocomposite Films Reinforced with Cellulose Nanocrystals: Rheology of Film-Forming Solutions, Transparency, Water Vapor Barrier and Tensile Properties of Films. *Carbohydr. Polym.* **2015**, *129*, 156–167. https://doi.org/10.1016/j.carbpol.2015.04.051.

(14) El Achaby, M.; El Miri, N.; Aboulkas, A.; Zahouily, M.; Bilal, E.; Barakat, A.; Solhy, A. Processing and Properties of Eco-Friendly Bio-Nanocomposite Films Filled with Cellulose Nanocrystals from Sugarcane Bagasse. *Int. J. Biol. Macromol.* **2017**, *96*, 340–352. https://doi.org/10.1016/j.ijbiomac.2016.12.040.

(15) Teixeira, E. de M.; Bondancia, T. J.; Theodore, K.B. R.; Corrêa, A.C.; Marconcini, J.M.; Mattoso, L. H.C. Sugarcane Bagasse Whiskers: Extraction and Characterizations. *Ind. Prod Crops.* **2011**, *33* (1), 63–66. https://doi.org/10.1016/j.indcrop.2010.08.009.

(16) Leo, R.M.; Mileo, P.C.; Maia, J.M. L.L.; Luz, S.M. Environmental and Technical Feasibility of Cellulose Nanocrystal Manufacturing from Sugarcane Bagasse. *Carbohydr. Polym.* **2017**, *175*, 518–529. https://doi.org/10.1016/j.carbpol.2017.07.087.

(17) Mandal, A.; Chakrabarty, D. Studies on the Mechanical, Thermal, Morphological and Barrier Properties of Nanocomposites Based on Poly(Vinyl Alcohol) and Nanocellulose from Sugarcane Bagasse. *J. Chem.* **2014**, *20* (2), 462–473. https://doi.org/10.1016/j.jiec.2013.05.003.

(18) Lam, N. T.; Chollakup, R.; Smitthipong, W.; Nimchua, T.; Sukyai, P. Utilizing Cellulose from Sugarcane Bagasse Mixed with Poly(Vinyl Alcohol) for Tissue Engineering Scaffold Fabrication. *Ind. Prod Crops.* **2017**, *100*, 183–197. https://doi.org/10.1016/j.indcrop.2017.02.031.

(19) Slavutsky, A.M.; Bertuzzi, M. A. Water Barrier Properties of Starch Films Reinforced with Cellulose Nanocrystals Obtained from Sugarcane Bagasse. *Carbohydr. Polym.* **2014**, *110*, 53–61. https://doi.org/10.1016/j.carbpol.2014.03.049.

(20) Ghaderi, M.; Mousavi, M.; Yousefi, H.; Labbafi, M. All-Cellulose Nanocomposite Film Made from Bagasse Cellulose Nanofibers for Food Packaging Application. *Carbohydr. Polym.* **2014**, *104* (1), 59–65. https://doi.org/10.1016/j.carbpol.2014.01.013.

(21) Li, J.; Wang, Y.; Wei, X.; Wang, F.; Han, D.; Wang, Q.; Kong, L. Homogeneous Isolation of Nanocelluloses by Controlling the Shearing Force and Pressure in Microenvironment. *Carbohydr. Polym.* **2014**, *113*, 388–393. https://doi.org/10.1016/j.carbpol.2014.06.085.

(22) Teixeira, R. S. S.; Da Silva, A. S. A.; Jang, J.H.; Kim, H.W.; Ishikawa, K.; Endo, T.; Lee, S.H.; Bon, E. P. S. Combining Biomass Wet Disk Milling and Endoglucanase/β-Glucosidase Hydrolysis for the Production of Cellulose Nanocrystals. *Carbohydr. Polym.* **2015**, *128*, 75–81. https://doi.org/10.1016/j.carbpol.2015.03.087.

(23) Campos, A. De; Carolina, A.; David, C.; Eliangela, C.́ and Sugarcane Bagasse Obtaining Nanofibers from Curaua Fibers Using Enzymatic Hydrolysis Followed by Sonication. **2013**. https://doi.org/10.1007/s10570-013-9909-3.

(24) Santucci, B. S.; Bras, J.; Belgacem, M. N.; Curvelo, A.A. da S.; Pepper, M. T.B. Evaluation of the Effects of Chemical Composition and Refining Treatments on the Properties of Nanofibrillated Cellulose Films from Sugarcane Bagasse. *Ind. Prod Crops.* **2016**, *91*, 238–248. https://doi.org/10.1016/j.indcrop.2016.07.017.

(25) Oksman, K.; Aitomäki, Y.; Mathew, A.P.; Siqueira, G.; Zhou, Q.; Butyline, S.; Tanpichai, S.; Zhou, X.; Hooshmand, S. Review of the Recent Developments in Cellulose Nanocomposite Processing. *Composed. Part A Appl. Sci. Manuf.* **2016**, *83*, 2–18. https://doi.org/10.1016/j.compositesa.2015.10.041.

(26) Abdul Khalil, H. P. S.; Davoudpour, Y.; Islam, M. N.; Mustapha, A.; Sudesh, K.; Dungani, R.; Jawaid, M. Production and Modification of Nanofibrillated Cellulose Using Various Mechanical Processes: A Review. *Carbohydr. Polym.* **2014**, *99*, 649–665. https://doi.org/10.1016/j.carbpol.2013.08.069.

(27) Bayer, T.; Cunning, B.V.; Selyanchyn, R.; Nishihara, M.; Fujikawa, S.; Sasaki, K.; Lyth, S.M. High Temperature Proton Conduction in Nanocellulose Membranes: Paper Fuel Cells. *Chem. Mater.* **2016**, *28* (13), 4805–4814. https://doi.org/10.1021/acs.chemmater.6b01990.

(28) Gadim, T.D.O.; Vilela, C.; Laurel, F. J. A.; Silvestre, A. J. D.; Freire, C. S. R.; Figueiredo, F.M. L. Nafion® and Nanocellulose: A Partnership for Greener Polymer Electrolyte Membranes. *Ind. Prod Crops.* **2016**, *93*, 212–218. https://doi.org/10.1016/j.indcrop.2016.01.028.

(29) Noonan, C.; Tajvidi, M.; Tayeb, A.H.; Shahinpoor, M.; Tabatabaie, S. E. Structure-Property Relationships in Hybrid Cellulose Nanofibrils/Nafion-Based Ionic Polymer-Metal Composites. *Materials (Basel).* **2019**, *12* (8), 7–9. https://doi.org/10.3390/ma12081269.

(30) Jiang, G. P.; Zhang, J.; Qiao, J.L.; Jiang, Y.M.; Zarrin, H.; Chen, Z.; Hong, F. Bacterial Nanocellulose/Nafion Composite Membranes for Low Temperature Polymer Electrolyte Fuel Cells. *J. Power Sources* **2015**, *273*, 697–706. https://doi.org/10.1016/j.jpowsour.2014.09.145.

(31) Hasani-Sadrabadi, M.M.; Dashtimoghadam, E.; Nasseri, R.; Karkhaneh, A.; Majedi, F.S.; Mokarram, N.; Renaud, P.; Jacob, K. I. Cellulose Nanowhiskers to Regulate the Microstructure of Perfluorosulfonate Ionomers for High-Performance Fuel Cells. *J. Mater. Chem. To* **2014**, *2* (29), 11334–11340. https://doi.org/10.1039/c4ta00635f.

(32) Larminie, J.; Dicks, A. *Fuel Cell Systems Explained*; Wiley: Chichester, 2003.

(33) Bagotsky, V.S. *Fuel Cells: Problems and Solutions.* , WILEY.; John Wiley & Sons: New Jersey, 2012. https://doi.org/10.1002/9780470432204.

(34) Yee, R. S.L.; Rozendal, R. A.; Zhang, K.; Ladewig, B. P. Cost Effective Cation Exchange Membranes: A Review. *Chem. Eng. Res. Des.* **2012**, *90* (7), 950–959. https://doi.org/10.1016/j.cherd.2011.10.015.

(35) University of Maine. *Product specification*. Available in: <https://umaine.edu/pdc/wp-content/uploads/sites/398/2016/03/Specs-CNC.pdf>. Accessed: 01, September, 2019.

(36) Dai, J.; Teng, X.; Song, Y.; Ren, J. Effect of Casting Solvent and Annealing Temperature on Recast Nafion Membranes for Vanadium Redox Flow Battery. *J. Memb. Sci.* **2017**, *522*, 56–67. https://doi.org/10.1016/j.memsci.2016.09.014.

(37) Klemm, D.; Kramer, F.; Moritz, S.; Lindström, T.; Ankerfors, M.; Gray, D.; Dorris, A. Nanocelluloses: A New Family of Nature-Based Materials. *Angew. Chemie - Int. Ed.* **2011**, *50* (24), 5438–5466. https://doi.org/10.1002/anie.201001273.

(38) Camarero Espinosa, S.; Kuhnt, T.; Foster, E. J.; Weder, C. Isolation of Thermally Stable Cellulose Nanocrystals by Phosphoric Acid Hydrolysis. *Biomacromolecules* **2013**, *14* (4), 1223–1230. https://doi.org/10.1021/bm400219u.

(39) American Society for Testing and Materials (ASTM). D 882-18: Standard Test Method for Tensile Properties of Thin Plastic Sheeting. 2018.

(40) Carmo, M.; Fritz, D.L.; Mergel, J.; Stolten, D. A Comprehensive Review on PEM Water Electrolysis. *Int. J. Hydrogen Energy* **2013**, *38* (12), 4901–4934. https://doi.org/10.1016/j.ijhydene.2013.01.151.

(41) Liang, Z.; Chen, W.; Liu, J.; Wang, S.; Zhou, Z.; Li, W.; Sun, G.; Xin, Q. FT-IR Study of the Microstructure of Nafion® Membrane. *J. Memb. Sci.* **2004**, *233* (1–2), 39–44. https://doi.org/10.1016/j.memsci.2003.12.008.

(42) Xu, W.; Lu, T.; Liu, C.; Xing, W. Low Methanol Permeable Composite Nafion/Silica/PWA Membranes for Low Temperature Direct Methanol Fuel Cells. *Electrochim. Act* **2005**, *50* (16–17), 3280–3285. https://doi.org/10.1016/j.electacta.2004.12.014.

(43) Neto;, W. P. F.; Alves, H.; Oliveira, N.; Pasquini, D. Extraction and Characterization of Cellulose Nanocrystals from Agro-Industrial Residue – Soy Hulls. *Ind. Crop. Prod.* **2013**, *42*, 480–488. https://doi.org/10.1016/j.indcrop.2012.06.041.

(44) New, L. P.; Bras, J.; García, A.; Belgacem, N.; Curvelo, A. A. S. Subcritical Water: A Method for Green Production of Cellulose Nanocrystals. *Acs sustain. Chem. Eng.* **2015**, *3* (11), 2839–2846. https://doi.org/10.1021/acssuschemeng.5b00762.

(45) Schroeder, L. R.; Gentile, V.M.; Atalla, R. H. Nondegradative Preparation of Amorphous Cellulose. *J. Chem Wood. Technol.* **1986**, *6* (1), 1–14. https://doi.org/10.1080/02773818608085213.

(46) Garvey, C. J.; Parker, I.H.; Simon, G. P. On the Interpretation of X-Ray Diffraction Powder Patterns in Terms of the Nanostructure of Cellulose I Fibres. **2005**, 1568–1575. https://doi.org/10.1002/macp.200500008.

(47) Rubatat, L.; Gebel, G.; Diat, O. Fibrillar Structure of Nafion: Matching Fourier and Real Space Studies of Corresponding Films and Solutions. *Macromolecules* **2004**, *37* (20), 7772–7783. https://doi.org/10.1021/ma049683j.

(48) Varanasi, S.; Henzel, L.; Mendoza, L.; Prathapan, R.; Batchelor, W.; Tabor, R.; Garnier, G. Pickering Emulsions Electrostatically Stabilized by Cellulose Nanocrystals. *Front. Chem.* **2018**, *6* (September), 1–9. https://doi.org/10.3389/fchem.2018.00409.

(49) Lin, M.; Singh Raghuwanshi, V.; Browne, C.; Simon, G.P.; Garnier, G. Modulating the Chiral Nanoarchitecture of Cellulose Nanocrystals through Interaction with Salts and Polymer. *J. Colloid Sci Interface.* **2022**, *613*, 207–217. https://doi.org/10.1016/j.jcis.2021.12.182.

(50) Matos, B. R.; Aucó, E.M.; Linardi, M.; Ferlauto, A.S.; Santiago, E. I.; Fonseca, F.C. Thermal Properties of Nafion-TiO2 Composite Electrolytes for PEM Fuel Cell. *J. therm. Anal. Calorim.* **2009**, *97* (2), 591–594. https://doi.org/10.1007/s10973-009-0365-0.

(51) Erbas Kiziltas, E.; Kiziltas, A.; Bollin, S.C.; Gardner, D. J. Preparation and Characterization of Transparent PMMA-Cellulose-Based Nanocomposites. *Carbohydr. Polym.* **2015**, *127*, 381–389. https://doi.org/10.1016/j.carbpol.2015.03.029.

(52) Dias, D. T.; Lopes, G.; Ferreira, T.; Oliveira, I. L.; Rosa, C. D. Thermo-Optical Properties of Perfluorinated Sulfonic Acid Membranes : An Investigation of Hydration Based on Absorption Spectra. **2017**, *71* (11), 2504–2511. https://doi.org/10.1177/0003702817723649.

(53) Matos, B. R.; Isidore, R. A.; Santiago, E. I.; Tavares, A.C.; Ferlauto, A.S.; Muccillo, R.;

Fonseca, F.C. Nafion-Titanate Nanotubes Composites Prepared by in Situ Crystallization and Casting for Direct Ethanol Fuel Cells. *Int. J. Hydrogen Energy* **2015**, *40* (4), 1859–1867. https://doi.org/10.1016/j.ijhydene.2014.11.102.

(54) Cele, N.; Ray, S. S. Recent Progress on Nafion-Based Nanocomposite Membranes for Fuel Cell Applications. *Macromol. Mater. Eng.* **2009**, *294* (11), 719–738. https://doi.org/10.1002/mame.200900143.

(55) Diloreto, E.; Haque, E.; Berman, A.; Moon, R. J. Freeze Dried Cellulose Nanocrystal Reinforced Unsaturated Polyester Composites : Challenges and Potential. *Cellulose* **2019**, *1*. https://doi.org/10.1007/s10570-019-02377-1.

(56) Hosseinpour, M.; Sahoo, M.; Perez-Page, M.; Baylis, S.R.; Patel, F.; Holmes, S.M. Improving the Performance of Direct Methanol Fuel Cells by Implementing Multilayer Membranes Blended with Cellulose Nanocrystals. *Int. J. Hydrogen Energy* **2019**, *44* (57), 30409–30419. https://doi.org/10.1016/j.ijhydene.2019.09.194.

(57) Chemours. *Product Information: Nafion N115, N117, N1110*; 2016.

(58) Gebel, G. Structural Evolution of Water Swollen Perfluorosulfonated Ionomers from Dry Membrane to Solution. *Polymer (Guildf).* **2000**, *41* (15), 5829–5838. https://doi.org/10.1016/S0032-3861(99)00770-3.

(59) Tayeb, A.H.; Amini, E.; Ghasemi, S.; Tajvidi, M. Cellulose Nanomaterials-Binding Properties and Applications: A Review. *Molecules* **2018**, *23* (10), 1–24. https://doi.org/10.3390/molecules23102684.

(60) Anderson, S. R.; Esposito, D.; Gillette, W.; Zhu, J.Y.; Baxa, U.; McNeil, S. E. Enzymatic Preparation of Nanocrystalline and Microcrystalline Cellulose. *J. Tappi.* **2014**, *13* (5), 35–42.

This preprint was submitted under the following conditions:

- The authors declare that they are aware that they are solely responsible for the content of the preprint and that the deposit in SciELO Preprints does not mean any commitment on the part of SciELO, except its preservation and dissemination.
- The authors declare that the necessary Terms of Free and Informed Consent of participants or patients in the research were obtained and are described in the manuscript, when applicable.
- The authors declare that the preparation of the manuscript followed the ethical norms of scientific communication.
- The authors declare that the data, applications, and other content underlying the manuscript are referenced.
- The deposited manuscript is in PDF format.
- The authors declare that the research that originated the manuscript followed good ethical practices and that the necessary approvals from research ethics committees, when applicable, are described in the manuscript.
- The authors declare that once a manuscript is posted on the SciELO Preprints server, it can only be taken down on request to the SciELO Preprints server Editorial Secretariat, who will post a retraction notice in its place.
- The authors agree that the approved manuscript will be made available under a Creative Commons CC-BY license.
- The submitting author declares that the contributions of all authors and conflict of interest statement are included explicitly and in specific sections of the manuscript.
- The authors declare that the manuscript was not deposited and/or previously made available on another preprint server or published by a journal.
- If the manuscript is being reviewed or being prepared for publishing but not yet published by a journal, the authors declare that they have received authorization from the journal to make this deposit.
- The submitting author declares that all authors of the manuscript agree with the submission to SciELO Preprints.